Mapping charge transfers between quantum levels using noncontact atomic force microscopy

Ł. Borowik, K. Kusiaku, D. Deresmes, D. Théron, H. Diesinger, and T. Mélin*
Institut d'Electronique de Microélectronique et de Nanotechnologie, CNRS-UMR 8520, Avenue Poincaré, BP 60069, 59652 Villeneuve d'Ascq Cedex, France

T. Nguyen-Tran and P. Roca i Cabarrocas
Laboratoire de Physique des Interfaces et des Couches Minces, CNRS-UMR 7647, Ecole Polytechnique, 91128 Palaiseau Cedex, France
(Received 14 June 2010; revised manuscript received 8 July 2010; published 6 August 2010)

We demonstrate the possibility to map nanoscale charge transfers between quantum electronic levels at room temperature, using noncontact atomic force microscopy and Kelvin force microscopy in a regime of weak electromechanical coupling. A two-level system is studied, consisting of degenerately doped silicon nanocrystals on silicon substrates, with size in the 2–50 nm range, in which the energy spacing is tuned by the nanocrystal quantum confinement over a ≈ 1 eV range. The nanocrystal ionization is found to follow an energy compensation mechanism driven by quantum confinement, in quantitative agreement with parametrized tight-binding calculations of its band structure.

DOI: 10.1103/PhysRevB.82.073302 PACS number(s): 73.22.−f, 07.79.Lh, 81.07.Ta

Measuring charging phenomena at the nanoscale is of fundamental interest in nanoscience. For example, charge displacements or dipolar interactions play a major role in chemistry and in self-assemblies, and thus drive bottom-up synthetic approaches in nanoscience. Also, the understanding of the charging spectrum of nanostructures, or of charge separation processes in functional materials is a key issue to build, e.g., single-electron or photovoltaic devices. So far, such issues have been investigated mostly using scanning-tunneling spectroscopy, enabling to explore for example the quantized electronic levels of molecules or nanocrystals,[1] as well as to map quantum wave functions in confined systems.[2]

An actual challenge consists in probing the charging spectrum of nanostructures or molecules with an atomic force microscope, i.e., from their electromechanical coupling to a cantilever tip probe. The advantage is that this "currentless" principle also holds on insulators, and is thus consistent with future nanotechnology applications. Recent work using noncontact atomic force microscopy (nc-AFM) have demonstrated single-charge detection of individual adatoms with a sub-nm resolution in vacuum and at 5 K.[3] The charging spectrum of nanocrystals has also been measured, at 5 K, in a regime of strong electromechanical coupling in which nanocrystal elementary charge jumps are observed upon electrical bias.[4,5]

In this Report, we address *at room temperature* the issue of mapping surface charge transfers between quantum levels. To do so, we investigate a quasi-two-level system consisting of degenerately doped silicon nanocrystals[6] on doped silicon substrates, with size in the 2–50 nm range. Charge transfers occur owing to the difference between the nanocrystal and substrate Fermi levels. Here, this energy difference is governed by quantum confinement induced by the nanocrystal size, and can be tuned over a ≈ 1 eV range. Charge transfers are investigated in a regime of weak electromechanical coupling using combined nc-AFM and Kelvin Force Microscopy (KFM),[7] and are analyzed quantitatively.[8] We demonstrate that the nanocrystal ionization follows an energy compensation mechanism enhanced by quantum confinement, in quantitative agreement with parametrized tight-binding calculations of the nanocrystal band structure.[9] This puts forward nc-AFM and KFM as tools to map charge transfers between quantum levels at the nanoscale.

Silicon nanocrystals have been fabricated by plasma enhanced chemical vapor deposition using silane (SiH_4) as silicon source and phosphine (PH_3) as phosphorus source for *n*-type doping during the plasma growth. Growth details are provided in Ref. 10. The samples studied in this work consist both (*i*) in reference samples, i.e., nominally undoped (intrinsic) nanocrystals collected from the plasma chamber on *p* or *n*-type silicon substrates ; and (*ii*) in *n*-type doped nanocrystals, deposited on *n*-type silicon substrates. *n* and *p* substrates have resistivities in the range of $0.001-0.006\ \Omega.\mathrm{cm}$ and $0.03-1\ \Omega.\mathrm{cm}$, respectively. Reference samples will be hereafter labeled *i*-NC/*n*-Si and *i*-NC/*p*-Si, respectively, while the doped nanocrystal samples on *n*-type wafers will be termed *n*-NC/*n*-Si. Three *n*-NC/*n*-Si samples S_1, S_2, and S_3 have been prepared, with PH_3 to SiH_4 flux ratios of 1/250, 1/50 and 1/25, respectively, leading to degenerate doping in the range of $\approx 10^{20}-10^{21}\ \mathrm{cm}^{-3}$.[11] To minimize the influence of surface states, all samples have been hydrogen-passivated in a diluted HF solution and rinsed in deionized water, before being loaded in the nc-AFM chamber (VT-AFM, Omicron Nanotechnology) operating at a base pressure of 10^{-10} mbar.

The charge state of nanocrystals is probed with a homemade Amplitude-Modulation Kelvin probe (AM-KFM) set up interfaced with a Nanonis controller (SPECS Zürich).[12] We used metal-plated cantilever tips (EFM PPP, Nanosensors) with 25 nm apex radius, and low resonance frequency ($f_0 \simeq 70$ kHz) and stiffness ($\simeq 3\ \mathrm{N\ m}^{-1}$). The resonance at f_0 is mechanically excited to perform nc-AFM topography with a detuning $\Delta f = -5$ Hz, and a typical tip-substrate distance $z = 20$ nm (15 ± 1 nm oscillation amplitude and 5 ± 1 nm minimum tip-substrate distance). The first cantilever harmonic at $f_1 = 6.2 f_0 \simeq 450$ kHz is simultaneously electrostatically excited with a $V_{dc} + V_{ac} \sin(2\pi f_1 t)$ voltage ($V_{ac} = 100$ mV) to acquire the KFM data. Noting $C(z)$ the tip-sample capacitance, the AM-KFM loop measures the surface potential V_S by regulating the value of V_{dc} so as to

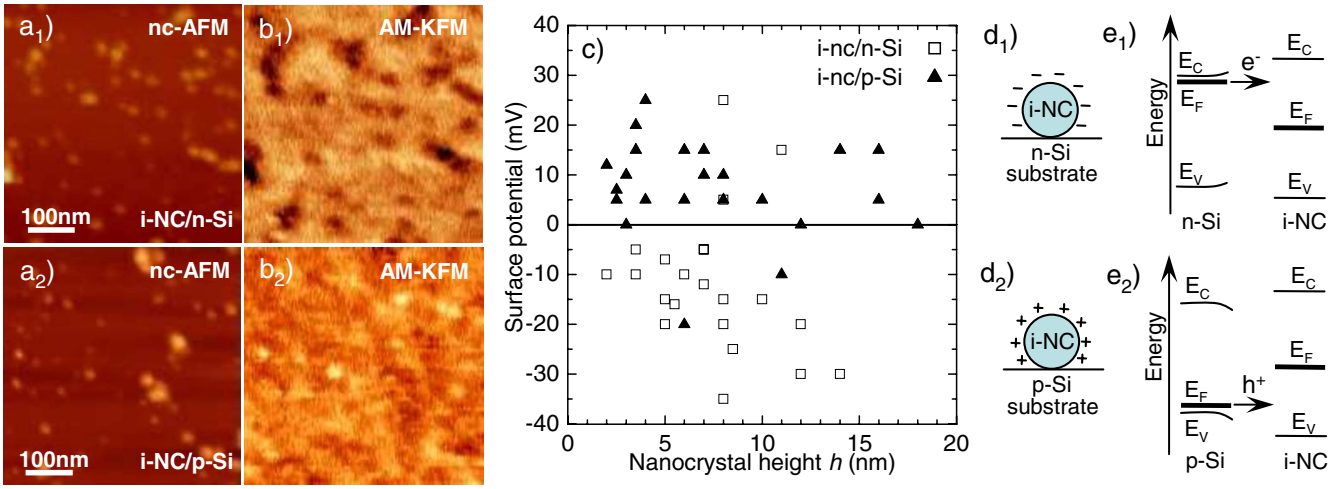

FIG. 1. (Color online) (a_1) and (a_2) 500×500 nm^2 noncontact atomic force microscopy image of hydrogen-passivated intrinsic nanocrystal samples on n-type and p-type doped wafers. The z-scale is 40 nm. (b_1) and (b_2) Simultaneously recorded amplitude-modulation Kelvin Force Microscopy images. The surface potential scale is 65 mV. (c) Plot of the surface potentials for the i-NC/n-Si and i-NC/p-Si samples, as a function of the nanocrystal height. (d_1) and (d_2) Schematics of the charging of the nanocrystal surface states (see text). (e_1) and (e_2) Corresponding energy diagrams prior to charge transfer indicated by the arrows.

maintain at zero the cantilever oscillation amplitude at f_1, which is proportional to $dC/dz(V_{dc}-V_S)\times V_{ac}$. The actual nanocrystal electrostatic potential is then extracted from experimental surface potentials, using a recently developed model[8] taking into account side-capacitance[13] and nonlinear effects associated with the tip oscillation.

We first start by describing experimental results obtained on the intrinsic reference samples (i-NC/n-Si and i-NC/p-Si). Simultaneously acquired nc-AFM and AM-KFM images are shown for both samples in Figs. 1(a) and 1(b), respectively. The upper (resp. lower) images and schematics in Fig. 1 correspond to the i-NC/n-Si and i-NC/p-Si samples. On Fig. 1(b) one can see that nanocrystals appear—*in average*—respectively, as dark features (negative potential) and bright features (positive potential) on n-Si and p-Si, corresponding to negative and positive charge states. This is further illustrated in Fig. 1(c), in which the KFM signals are plotted as a function of the nanocrystal height h. KFM signals do not appear correlated with h, but exhibit rather strong fluctuations. We interpret this effect qualitatively as the charging of the nanocrystal surface states by the substrate free carriers. This is schematically illustrated in Figs. 1(d_1) and 1(d_2), assuming the defects to be localized on the nanocrystal surface. The corresponding energy diagrams are shown in Fig. 1(e_1) and 1(e_2) for the i-NC/n-Si and i-NC/p-Si samples, respectively. The hydrogen-passivated Si substrate is here represented with a Fermi level pinned close to the bands at the semiconductor-vacuum interface. The sign of the charge transfer is governed by the difference between the Fermi levels of the substrate and nanocrystals, as shown in Figs. 1(e_1) and 1(e_2). This picture accounts for the negative (respectively, positive) charge transfer and surface potentials observed—*in average*—for the i-NC/n-Si and i-NC/p-Si samples, and for the surface potential fluctuations [Fig. 1(c)] due to the variation of the actual Fermi level position in the nanocrystals related to surface or defect states, in spite of the hydrogen passivation.

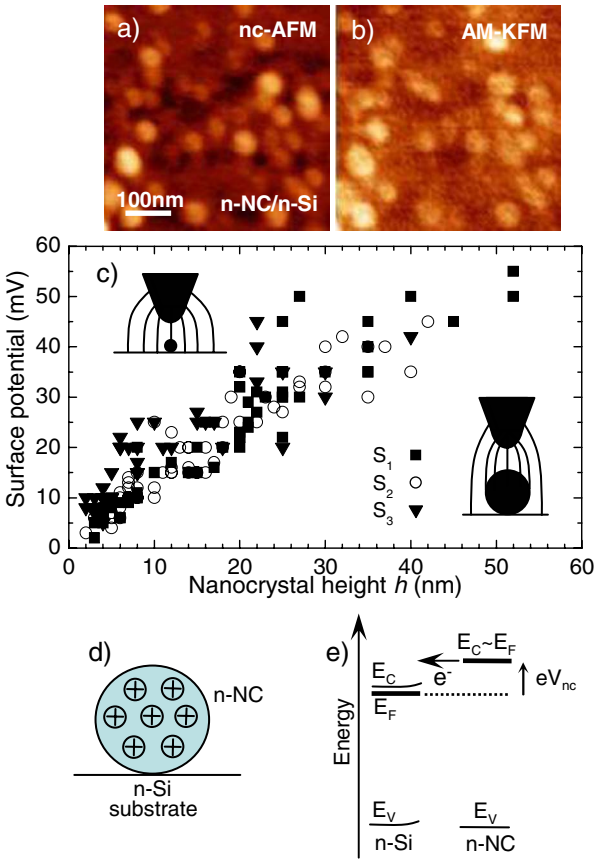

FIG. 2. (Color online) (a) 500×500 nm^2 nc-AFM image (40 nm z-scale) and (b) AM-KFM image (70 mV potential scale) of the n-NC/n-Si sample S_2. (c) KFM surface potentials as a function of the nanocrystal height h for the three samples S_1, S_2 and S_3. (d) Schematics of the ionized nanocrystal. (e) Energy diagram prior to the charge transfer (indicated by the arrow). Insets: schematics of side-capacitance effects in KFM, leading to the averaging of the electrostatic potential for small nanocrystals.

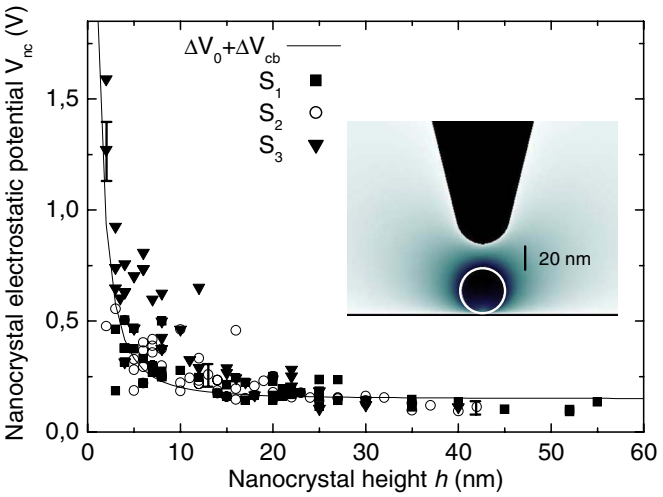

FIG. 3. (Color online) Nanocrystal electrostatic potentials of samples S_1, S_2, and S_3 as a function of their height h, assuming a spherical geometry (see inset). The line corresponds to $\Delta V_0+\Delta V_{cb}$, in which ΔV_{cb} accounts for quantum confinement and $\Delta V_0=150$ mV in spherical geometry. Error bars correspond to the uncertainty in calculations with respect to tip-shape modeling (see text).

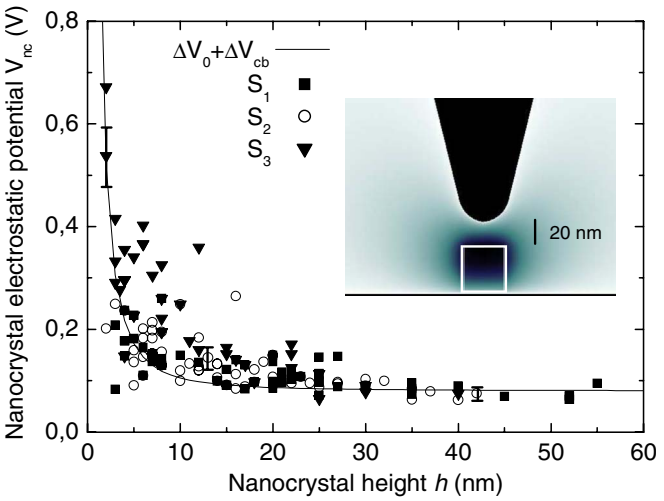

FIG. 4. (Color online) Same plot as in Fig. 3, but using an assumption of cylindrical shape in calculations made to extract the ionized nanocrystal electrostatic potential from experimental KFM data. The line corresponds to $\Delta V_0+\Delta V_{cb}$, here with ΔV_{cb} in cylindrical geometry (see text) and $\Delta V_0=80$ mV.

We now turn to the n-NC/n-Si samples. nc-AFM and AM-KFM images are shown in Figs. 2(a) and 2(b) (here for S_2), together with a plot of the KFM signals of S_1, S_2 and S_3 as a function of the nanocrystal height in Fig. 2(c). Remarkably, the nanocrystal surface potentials:

(i) are positive [Fig. 2(b)], in contrast with the i-NC/n-Si sample [Fig. 1(b_1)];

(ii) exhibit much smaller fluctuations [Fig. 2(c)] as compared to the i-NC/n-Si sample [Fig. 1(c)];

(iii) are identical for the samples S_1, S_2, and S_3 [Fig. 2(c)], in spite of their different nominal doping levels.

We ascribe the reduction of the KFM fluctuations to the internal passivation of the nanocrystal surface states or defects upon doping,[14] as pointed out in a recent work using electron paramagnetic resonance.[11] The positive nanocrystal charging is then understood as a partial ionization due to the transfer of free electrons toward the substrate, as sketched in Fig. 2(d). The corresponding energy diagram is shown in Fig. 2(e). An energy compensation mechanism is expected, in which the electrostatic energy of the ionized nanocrystals equilibrates the initial difference in Fermi energies. This accounts for the observation that the nanocrystal surface potentials are identical for the samples S_1, S_2, and S_3, in spite of their different nominal doping levels. This model also predicts a strong enhancement of the ionized nanocrystal electrostatic energy, due to the nanocrystal band-gap opening associated with quantum confinement [Fig. 2(e)].

To verify this, we extracted the actual nanocrystal electrostatic potential V_{nc} from KFM measurements, by correcting the experimental data from side capacitance effects [see insets in Fig. 2(c)] and nonlinear effects due to the tip oscillation in the combined nc-AFM and KFM mode. The principles and details of the calculations can be found in Ref. 8, and are therefore not detailed in this paper. Calculations enable to convert the surface potential values measured by KFM to the nanocrystal electrostatic potential V_{nc}, taking into account the tip scanning conditions (tip height and oscillation amplitude), and the tip/nanocrystal geometry. They are basically obtained from electrostatic force fields, using a commercial Poisson solver (COMSOL) in axial symmetry with a spherical-conical tip.[15] The ionized nanocrystals are treated as homogeneously charged dielectric nanoparticles.[16]

V_{nc} values extracted from experimental KFM data in a spherical nanocrystal geometry are shown in Fig. 3 (points) in which the error bars (10%) correspond to the maximum uncertainty in calculations while changing the tip-apex radius/tip-cone angles in the range of 20–30 nm and 8°–20°. V_{nc} is found almost constant for nanocrystals with large height $h \geq 25$ nm ($\Delta V_0 \simeq 150$ mV). It however drastically increases while reducing the nanocrystal height h, and especially for $h \leq 10$ nm as expected from quantum confinement.

Results of Fig. 3 are compared with parametrized tight-binding calculations[9] of the conduction band energy shift ΔV_{cb} due to quantum confinement, using a spherical geometry assumption for the nanocrystals.[17] More precisely, we compare the electrostatic potential of the nanocrystals V_{nc} with $\Delta V_0+\Delta V_{cb}$, in which we fix ΔV_0 to the electrostatic potential observed for nanocrystals with negligible quantum confinement, which can be attributed to the nominal difference of the nanocrystal and substrate Fermi levels. The values of $\Delta V_0+\Delta V_{cb}$ (line in Fig. 3) are seen to remarkably fit to the nanocrystal electrostatic potentials *without any adjustable parameter*. This identifies the raise of electrostatic potential at small diameters as stemming from quantum confinement.

Since nc-AFM measurements only provide a precise information about the nanocrystal height but not their precise shape due to tip convolution, we demonstrate additionally that the above analysis is robust with respect to the assumption of the nanocrystal geometry. Therefore, and although the nanocrystals are in reality close to spheres,[10] we performed again the numerical extraction of the nanocrystal electro-

static potential V_{nc} from the experimental KFM data,[8] here however in a cylindrical geometry, with equal cylinder height and base diameter (see inset in Fig. 4). Results are plotted in Fig. 4 and compared with $\Delta V_0+\Delta V_{cb}$, in which $\Delta V_0=80$ mV and ΔV_{cb} is plotted for a cylindrical geometry as well.[17] An excellent agreement is again found, demonstrating that the enhancement in ΔV_{nc} is not related to a geometry assumption for the nanocrystals, but quantitatively fits quantum-mechanical expectations of Ref. 9.

We finally comment on the nanocrystal ionization charge as a function of the nanocrystal height. In a spherical geometry, and assuming an homogeneous charge distribution,[16] the volume ionization of the nanocrystals corresponds to a power-law behavior in $h^{-\alpha_V}$ with $\alpha_V=2.7$ close to 3, together with variations in the $5\times10^{17}-1\times10^{21}$ cm^{-3} range. We measured the maximum volume charge densities for the three samples, which show a gradation for S_1, S_2 and S_3 in the range $10^{20}-10^{21}$ cm^{-3}. Assuming a full ionization regime (here corresponding to a single-electron detection limit), this provides a measurement of the nanocrystal doping level. Such densities fall remarkably in agreement with the doping levels expected from growth conditions,[11] although an actual measurement of the nanocrystal doping level would require a true statistical analysis.

In conclusion, we have addressed, at room temperature, the issue of mapping surface charge transfers between quantum levels using combined nc-AFM and KFM, from a two-level system consisting of degenerately doped silicon nanocrystals on doped silicon substrates. The nanocrystal ionization was found to follow an energy compensation mechanism driven by quantum confinement, in quantitative agreement with parametrized tight-binding calculations of the nanocrystal band structure. Our results put forward the use of noncontact atomic force microscopy and Kelvin force microscopy to map charge transfers beween quantum levels at the nanoscale.

We acknowledge fruitful discussions with C. Delerue.

*thierry.melin@isen.iemn.univ-lille1.fr

[1] See, e.g., U. Banin, Y. Cao, D. Katz, and O. Millo, Nature (London) **400**, 542 (1999).

[2] See, e.g., B. Grandidier, Y. M. Niquet, B. Legrand, J. P. Nys, C. Priester, D. Stiévenard, J. M. Gérard, and V. Thierry-Mieg, Phys. Rev. Lett. **85**, 1068 (2000); T. Maltezopoulos, A. Bolz, C. Meyer, C. Heyn, W. Hansen, M. Morgenstern, and R. Wiesendanger, *ibid.* **91**, 196804 (2003); S. Fölsch, P. Hyldgaard, R. Koch, and K. H. Ploog, *ibid.* **92**, 056803 (2004).

[3] L. Gross, F. Mohn, P. Liljeroth, J. Repp, F. J. Giessibl, and G. Meyer, Science **324**, 1428 (2009).

[4] R. Stomp, Y. Miyahara, S. Schaer, Q. Sun, H. Guo, P. Grütter, S. Studenikin, P. Poole, and A. Sachrajda, Phys. Rev. Lett. **94**, 056802 (2005).

[5] S. D. Bennett, L. Cockins, Y. Miyahara, P. Grütter, and A. A. Clerk, Phys. Rev. Lett. **104**, 017203 (2010).

[6] For a recent review, see: D. J. Norris, A. L. Efros, and S. C. Erwin, Science **319**, 1776 (2008); S. C. Erwin, L. Zu, M. I. Haftel, A. L. Efros, T. A. Kennedy, and D. J. Norris, Nature (London) **436**, 91 (2005), and references therein.

[7] For a seminal paper, see: Y. Martin, D. W. Abraham, and H. K. Wickramasinghe, Appl. Phys. Lett. **52**, 1103 (1988).

[8] Ł. Borowik, K. Kusiaku, D. Théron, and T. Mélin, Appl. Phys. Lett. **96**, 103119 (2010).

[9] Y. M. Niquet, C. Delerue, G. Allan, and M. Lannoo, Phys. Rev. B **62**, 5109 (2000).

[10] See: P. Roca i Cabarrocas, Th. Nguyen-Tran, Y. Djeridane, A. Abramov, E. Johnson, and G. Patriarche, J. Phys. D **40**, 2258 (2007).

[11] A. R. Stegner, R. N. Pereira, K. Klein, R. Lechner, R. Dietmueller, M. S. Brandt, M. Stutzmann, and H. Wiggers, Phys. Rev. Lett. **100**, 026803 (2008); R. Lechner, A. R. Stegner, R. N. Pereira, R. Dietmueller, M. S. Brandt, A. Ebbers, M. Trocha, H. Wiggers, and M. Stutzmann, J. Appl. Phys. **104**, 053701 (2008).

[12] A detailed description of our set-up can be found in: H. Diesinger, D. Deresmes, J. P. Nys, and T. Mélin, Ultramicroscopy **110**, 162 (2010).

[13] H. O. Jacobs, P. Leuchtmann, O. J. Homan, and A. Stemmer, J. Appl. Phys. **84**, 1168 (1998).

[14] This internal passivation mechanism generates an *unoriented* distribution of dipoles within the nanocrystals which shall not affect their surface potential, unlike for the *i*-NC/*n*-Si sample in which the net nanocrystal charge forms a dipole perpendicular to the substrate, see: T. Mélin, H. Diesinger, D. Deresmes, and D. Stiévenard, Phys. Rev. Lett. **92**, 166101 (2004).

[15] A cantilever is also introduced in simulations, with equivalent capacitance gradient as experimental cantilevers.

[16] This assumption would also correspond to the case of nanocrystals with core doping.

[17] We use here $\Delta V_{cb}=K_c/(h^2+a_ch+b_c)$, in which $(K_c;a_c;b_c)$, expressed in mV.nm, nm and nm^2, equal (5844.5; 1.274; 0.905) and (2811.6; 1.027; 0.396) respectively for silicon spheres and cylinders with height h.